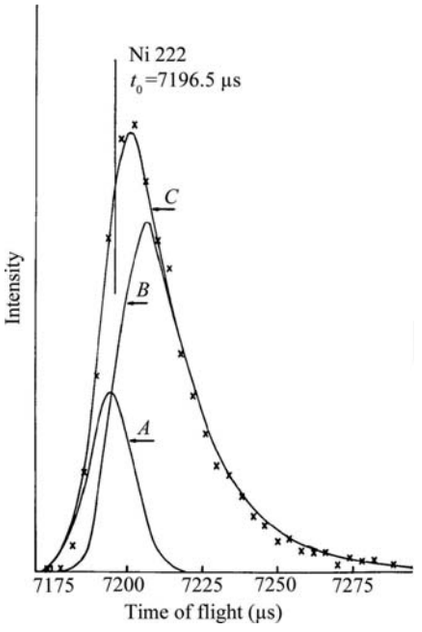

Figure 3.3.3
The observed and calculated Ni 222 diffraction line profile from the Back Scattering Spectrometer, Harwell Laboratory, Chilton, UK. The curves *A* and *B* are computed from the two terms in equation (3.3.19) and curve *C* is the sum (from Von Dreele *et al.*, 1982).

particularly for long-pulse sources, to give what is seen at the powder diffractometer.

Consequently, the neutron pulse structure from these sources has a complex and asymmetric shape, usually characterized by a very sharp rise and a slower decay, both of which are dependent on the neutron wavelength. The resulting powder diffraction peak profile (Fig. 3.3.3) is then the convolution [equation (3.3.2)] of this pulse shape (G_λ) with symmetric functions (G_I) arising from beamline components (*e.g.* slits and choppers) and the sample characteristics (G_S).

3.3.3.3. *The neutron TOF powder peak profile*

An early attempt at representing the TOF peak profile used a piecewise approach combining a leading-edge Gaussian, a peak-top Gaussian and an exponential decay for the tail (Cole & Windsor, 1980). Although single peaks could be fitted well with this function, the variation with TOF was complex and required many arbitrary coefficients.

A more successful approach empirically represented the pulse shape by a pair of back-to-back exponentials which were then convoluted with a Gaussian (Jorgensen *et al.*, 1978; Von Dreele *et al.*, 1982) to give

$$P(\Delta) = \frac{\alpha\beta}{\alpha+\beta}\left\{\exp\left[\frac{\alpha}{2}(\alpha\sigma^2+2\Delta)\right]\operatorname{erfc}\left[\frac{\alpha\sigma^2+\Delta}{\sigma(2^{1/2})}\right] + \exp\left[\frac{\beta}{2}(\beta\sigma^2-2\Delta)\right]\operatorname{erfc}\left[\frac{\beta\sigma^2-\Delta}{\sigma(2^{1/2})}\right]\right\}, \tag{3.3.19}$$

where α and β are, respectively, the coefficients for the exponential rise and decay functions; erfc is the complementary error function. Analysis of the data that were available then gave empirical relations for α, β and σ as

$$\alpha = \alpha_1/d; \quad \beta = \beta_0 + (\beta_1/d^4); \quad \sigma = \sigma_1 d. \tag{3.3.20}$$

The two terms in this function are shown in Fig. 3.3.3. The junction of the two exponentials defines the peak position (shown as a vertical line in Fig. 3.3.3); it is offset to the low side of the peak maximum. This arbitrary choice of peak position then affects the relationship between the TOF and reflection *d*-spacing; an empirical relationship (Von Dreele *et al.*, 1982) was found to suffice:

$$\mathrm{TOF} = Cd + Ad^2 + Z, \tag{3.3.21}$$

with three adjustable coefficients (C, A, Z) established *via* fitting to the pattern from a standard reference material.

Although this profile description was adequate for room-temperature moderators (H_2O or polyethylene) at low-power spallation sources, it does not describe well the wavelength dependence for cold moderators feeding neutron guides used at higher-power sources. An alternative description, employing a switch function to account for the fundamental change in the neutron leakage profile from the moderator between epithermal and thermal neutrons, was proposed (Ikeda & Carpenter, 1985; Robinson & Carpenter, 1990) to accommodate the profiles seen from liquid CH_4 or H_2 moderators. A drawback of this description is that the pulse profile is defined with the peak position at the low TOF edge; convolution with G_I and G_S results in a function where the peak position is far below the peak top. An empirical approach by Avdeev *et al.* (2007) simply requires tables to be established from individual peak fits to a standard material powder pattern for the values of α, β and TOF in place of the expressions given in equations (3.3.20) and (3.3.21); this establishes the G_λ and G_I contributions to the TOF line shape. More recently, some simple extensions (Toby & Von Dreele, 2013) to the empirical functions [equations (3.3.22) and (3.3.23)] appear to better cover the deviations arising from the enhanced epithermal contribution to the cold moderator spectrum:

$$\mathrm{TOF} = Cd + Ad^2 + B/d + Z, \tag{3.3.22}$$

$$\alpha = \frac{\alpha_1}{d}; \quad \beta = \beta_0 + \frac{\beta_1}{d^4} + \frac{\beta_2}{d^2}; \quad \sigma = \sigma_0 + \sigma_1 d^2 + \sigma_2 d^4 + \frac{\sigma_3}{d^2}. \tag{3.3.23}$$

3.3.4. Peak profiles for X-ray energy-dispersive experiments

In an X-ray dispersive powder diffraction experiment, a detector with good energy-discrimination capability is placed at a fixed scattering angle while the sample is illuminated by a 'white' beam of radiation. The detector response is binned into discrete energies by a multichannel analyser (MCA) (Glazer *et al.*, 1978). Typically these instruments display peaks that are purely Gaussian in shape with quite low resolution ($\Delta E/E \simeq 1\%$) and have widths that are proportional to the energy:

$$\Gamma_G = UE + W. \tag{3.3.24}$$

This is most useful for experiments with very limited angular access (*e.g.* high-pressure multi-anvil setups, as described in Chapter 2.7) using synchrotron radiation and can give very high data collection rates on very small samples. Glazer *et al.* (1978) showed that simple crystal structures can be modelled with the Rietveld technique after suitable corrections to account for the variation in source intensity, detector response and sample absorption effects. Otto (1997) expanded the peak-profile description to include possible sample-broadening effects *via* a Voigt profile; this extended the expression in equation (3.3.24) by adding a second-order term in energy and allowed extraction of